The Modulated Structure of LaMo₈O₁₄

By H. Leligny, P. Labbe, M. Ledesert, M. Hervieu and B. Raveau

Laboratoire CRISMAT, ISMRa, Bd du Maréchal Juin, 14050 Caen, France

and W. H. McCarroll

Chemistry Department, Rider College, POB 6400, Lawrence ¹/ᵉ, NJ 08648, USA

Abstract

Lanthanum octamolybdate [$LaMo_8O_{14}$, $a = 11.129$ (1), $b = 10.000$ (1), $c = 9.218$ (1) Å, basic space group $C2ca$, superspace group $P_{\bar{1}\bar{1}\bar{1}}^{C2ca}$, $M_r = 1130.4$, $D_x = 7.32$ g cm⁻³, $V = 1025.9$ Å³, $Z = 4$, $T = 294$ K, Mo $K\alpha$ radiation, $\lambda = 0.710730$ Å, $\mu = 134.5$ cm⁻¹, $F(000) = 2020$] exhibits a one-dimensional modulated structure that is found to be commensurate within experimental error with a modulation wavevector $\mathbf{q}^*$ having components $0,\frac{1}{3},0$. Both a density modulation wave, governing the occupancy probability of some atomic sites [La(1), La(2), Mo(4) and Mo(5)], and a displacive modulation wave of small but significant amplitude, acting on all atoms, are involved in the crystal. The modulated structure was refined from 3347 unique *hklm* reflections [$I \ge 3\sigma(I)$] with the *REMOS* program. The final R factors (based on F) of the (1845) main reflections and the (1502) first-order satellite reflections are 0.038 and 0.090, respectively. Because the q_2^* component of $\mathbf{q}^*$ has the particular value $\frac{1}{3}$ and the modulation is harmonic, remarkable relations result between the atomic displacements. Within a classical approach, with use of the space-group description, these relations would be masked. The average structure of this crystal appears to be closely related to the structure of $LaMo_{7.7}O_{14}$ crystal, which is not modulated. The main result of this study is the occurrence of four distinct configurations of the Mo_8 metallic clusters inside the same crystal. As suggested by the results of electron microscopy investigations, a more or less large deviation from an ideal structural order would be involved in most of the modulated crystals.

Introduction

Recently, we reported (Leligny, Ledesert, Labbe, Raveau & McCarroll, 1990) on the structure of $LaMo_{7.70}O_{14}$ which contains a bi-faced capped octahedron of bonded Mo atoms. This Mo_8 unit is of interest not only because it represents the first example of the *cis*-edge-sharing isomeric form of such clusters found in chemical systems but also because it is found as a fragment in various extended systems containing metal–metal bonds (Gougeon & McCarley, 1991). A second curious and unexplained feature was that the face-capping sites are only partially occupied, giving rise to a statistical mixture of Mo_8, Mo_7 and perhaps Mo_6 groups within the structure.

Shortly after the appearance of this paper, Gougeon & McCarley (1991) reported on the structure of $NdMo_8O_{14}$ and found that it was the fully stoichiometric analogue of $LaMo_{7.70}O_{14}$. They also mentioned that they were able to prepare apparently stoichiometric compounds by high-temperature solid-state reactions when Nd was replaced by La, Ce, Pm or Gd. In contrast, we prepared $LaMo_{7.70}O_{14}$ by the electrolytic technique described below. However, we were aware that some of the samples prepared by this method produced crystals exhibiting satellite reflections that were indicative of a modulation. Our studies have shown that the modulated crystal represents what is apparently a second form of fully stoichiometric $LaMo_8O_{14}$, the results of which are presented here.

Synthesis

The crystals were synthesized by the electrolysis of a melt having the composition $Na_2MoO_4:MoO_3:La_2O_3 = 3.50:3.50:1.00$ at 1353–1363 K. The reactions were carried out in air using a charge of 30 g contained in a McDanel 997 high-density alumina crucible. Electrolyses were carried out using Pt-foil electrodes (1 cm²) at a current density of 200 mA cm⁻² for periods of 1 to 1.5 h. The product, which grows at the cathode in the form of small black plates, was often intermixed with $La_{1+x}Mo_8O_{16}$, $La_9Mo_{13}Al_2O_{42}$ and sometimes coated with MoO_2. The first two compounds, because of their distinctive needle-like or prismatic habit, could easily be separated mechanically from the product of interest. A brief wash in

warm $4\,F\,HNO_3$ followed by a short wash in dilute HCl served to remove any MoO_2 present. Prior to this treatment, the reduced products were separated from the matrix by alternate washes in hot 5% potassium carbonate solution and hot $2\,F\,HCl$. It should be noted that this synthesis procedure differs from that used to prepare $LaMo_{7.70}Mo_8O_{14}$ only in a slightly higher range of temperatures and an increased current density. Furthermore, the procedure described here has sometimes yielded this latter compound exclusively in the form of heavily twinned intergrowths.

Preliminary study

X-ray diffraction photographs, recorded at room temperature with a Weissenberg camera, show both main reflections and satellite reflections defined by a single modulation wavevector $\mathbf{q}^* = q_2^*\mathbf{b}^*$ with q_2^* nearly equal to $\frac{1}{3}$. All the reflections conform to mmm Laue symmetry. As suggested by the study of the main reflections, the basic structure of this crystal, having the composition $LaMo_8O_{14}$, appears to be closely related to the structure of the orthorhombic crystal of composition $LaMo_{7.7}O_{14}$ (Leligny et al., 1990). Indeed, for the two phases, the lattice parameters are similar [$a_M = 11.129$ (1), $b_M = 10.000$ (1), $c_M = 9.218$ (1), $a = 11.171$ (1), $b = 9.985$ (1), $c = 9.196$ (1) Å, where M refers to the modulated crystal]. The intensities of the reflections of equivalent h,k,l indices are of the same magnitude and the systematic extinctions are identical. Unusual features are observed for the satellite reflections, which exhibit a large angular spread along the $[010]^*$ rows, in contrast with the main reflections, which are sharp. Moreover, these satellite reflections display asymmetric profiles and are merged in diffuse $[010]^*$ streaks of weak intensity. Satellite reflections of second order are not detected. As an example, the peak profiles of the 112 main reflection and of its two satellites are compared in Fig. 1. These profiles were determined with a CAD-4 Enraf–Nonius diffractometer through the measurement of the intensities i over the related intervals of the $\Delta\Omega$ scan angles. The angular width of the satellite reflections (defined by $i \geq i_{max}/2$), along $[010]^*$, is not constant but varies from about 0.6 to 0.9°, while that of the main reflections is nearly constant at 0.2°.

The cell parameters of the crystal were refined by least-squares techniques from the θ measurements of 20 main reflections ($18.57 \leq \theta \leq 30.63°$). Subsequently, to refine the q_2^* value, the θ_s angles of 20 satellite reflections were carefully measured on the basis of the supercell $\mathbf{a}$, $3\mathbf{b}$, $\mathbf{c}$ and then compared with the calculated ones corresponding to the hypothesis $q_2^* = \frac{1}{3}$. No systematic and significant discrepancies were found between the measured and

calculated θ_s values; consequently the rational value of $\frac{1}{3}$ was assumed for q_2^*.

A structural investigation based on the four-dimensional space-group approach was chosen over the classical method requiring a supercell for two main reasons: (i) from the viewpoint of the extinction rules, the superspace-group description leads to a better understanding of the diffraction pattern (van Smallen, 1987); (ii) the introduction of modulation functions to describe the distortion of the basic

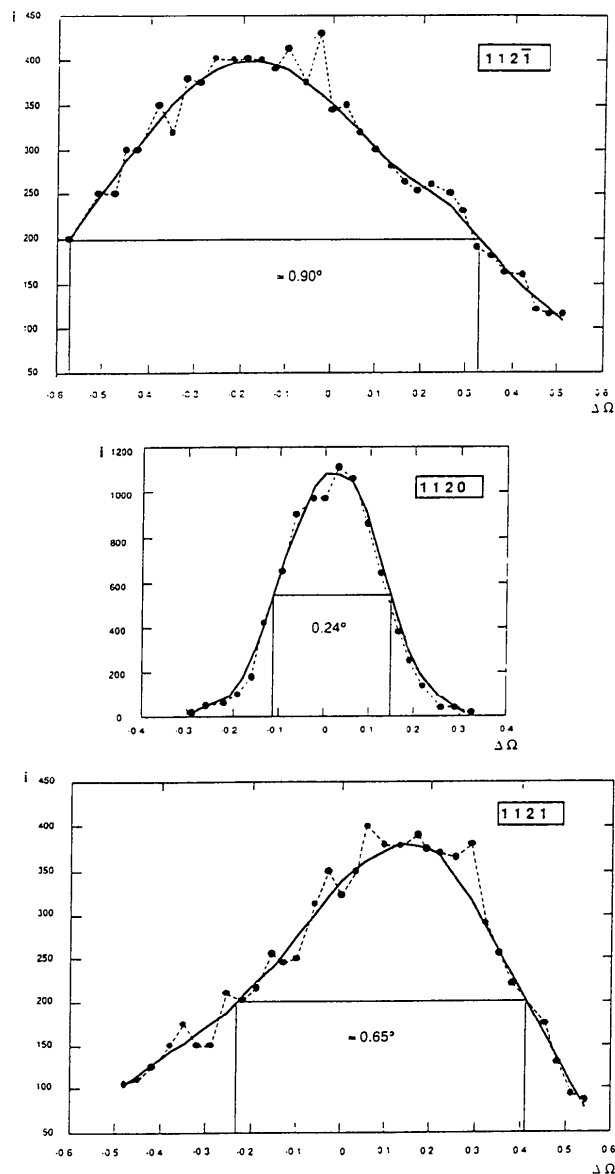
Fig. 1. A comparison of the profiles of the 1120 main reflection and of its two 112$\bar{1}$, 1121 satellites. These peak profiles were determined by measuring the intensity i (arbitrary units) as a function of $\Delta\Omega$. The angular width at half-maximum is indicated.

structure allows one to relate in a simple way the atomic displacements and the atomic site occupancies through the various cells of the actual crystal. Within this approach, all reflections are labelled with four h,k,l,m integers by definition of the diffraction vector as

$$\mathbf{s}^* = h\mathbf{a}^* + k\mathbf{b}^* + l\mathbf{c}^* + m\mathbf{q}^*,$$

where m is the satellite order. The reflection conditions

$$hklm, \quad h + k = 2n,$$
$$hk0m, \quad h = 2n \ (k = 2n),$$
$$h0l0 \quad l = 2n \ (h = 2n),$$

are consistent with the two superspace groups $P^{C2ca}_{\bar{1}\bar{1}\bar{1}}$ and $P^{Cmca}_{\bar{1}\bar{1}\bar{1}}$.

To determine the best conditions for gathering intensity data, preliminary investigations were carried out. Owing to the large angular spread of the satellite reflections, several scan modes were tested on a limited number of reflections to determine the optimal $\Delta\Omega$ range. The intensity measurement of a satellite reflection was taken to be valid if the left and the right background intensities were of similar magnitude. Meanwhile, a bias on some satellite intensities was expected since the background intensities could not be measured exactly along [010]* for all the reflections with the automatic scanning process. As several reflections have intensities equal to zero within the supercell description, the recording of the intensities with the diffractometer was performed with the *SAT* program (Doudin, 1985), which generates a file including the h,k,l,m and $R_h = h$, $R_k = k + mq_2^*$, $R_l = l$ indices.

The intensities of 3347 unique $hklm$ reflections (including 1502 satellite reflections of first order) with $I \geq 3\sigma(I)$ were corrected for Lorentz and polarization effects and used to refine the modulated structure. The absorption corrections, based on the crystal morphology, were applied within the *REMOS* program (Yamamoto, 1982). The main features of the data collection are summarized in Table 1.†

The average structure

The average structure was refined from the main reflections using the internal *SDP* programs (B. A. Frenz & Associates, Inc., 1982). The polar space group $C2ca$, used successfully to solve the structure of LaMo₇.₇O₁₄ shown in Fig. 2, was chosen. Let us

---

† Lists of structure factors have been deposited with the British Library Document Supply Centre as Supplementary Publication No. SUP 55746 (12 pp.). Copies may be obtained through The Technical Editor, International Union of Crystallography, 5 Abbey Square, Chester CH1 2HU, England.

Table 1. *Experimental data of* LaMo₈O₁₄

Crystal size	Plate, 232 × 116 × 64 μm
Lattice parameters (294 K)	$a = 11.129$ (1), $b = 10.000$ (1), $c = 9.218$ (1) Å
Modulation wavevector	$\mathbf{q}^*(0,\frac{1}{3},0)$
Modulation period	$\lambda = 1/q^* = 30$ Å
Superspace group	$P^{Cmca}_{\bar{1}\bar{1}\bar{1}}$
D_x, Z, M, V	7.32 (1) g cm⁻³, 4, 1130.4, 1025.9 (3) Å³
$F(000)$	2020
Data-collection technique	Enraf-Nonius CAD-4 diffractometer
Scan mode	ω, $\frac{4}{3}\theta$
Wavelength	λ(Mo $K\alpha$) = 0.710730 Å
$(\sin\theta/\lambda)_{max}$	0.995 Å⁻¹
Registered space	$0 \leq h \leq 22$, $0 \leq k \leq 19$, $0 \leq l \leq 18$, $-1 \leq m \leq 1$
Control of intensities	3000 s; no fluctuation
Number of measured reflections	7089
Number of reflections with $I \geq 3\sigma(I)$	1845 main reflections 1502 satellite reflections
Absorption correction	Based on the crystal morphology
Absorption coefficient	$\mu = 134.5$ cm⁻¹
Extremal transmission factors	0.43, 0.15
Atomic scattering factors and f', f'' values	From *International Tables for X-ray Crystallography* (1974, Vol. IV)

recall that within this structure the sites pseudo-equivalent to La(1) and Mo(4), by reflection in the yOz plane, are empty; moreover, the La(1) site is fully occupied while the Mo(4) site is partially occupied [0.848 (2)]. With the atomic positions of LaMo₇.₇O₁₄ crystal (Leligny *et al.*, 1990) as a starting point, Fourier difference synthesis showed two significant residual peaks located at remarkable positions related to those of the La(1) and Mo(4) sites through the yOz plane. The heights of the two residual peaks corresponded roughly to $\frac{1}{6}$ La and $\frac{1}{5}$ Mo respectively. This result suggests that the La atom is distributed, with different probabilities, over two pseudoequivalent sites labelled La(1) and La(2) in Fig. 3, which shows a partial (001) plane projection of the average structure. A similar phenomenon occurs for the Mo atoms over the sites labelled Mo(4) and Mo(5) in Fig. 3. Several refinement cycles were then carried out with the previous features taken into account; no constraints were applied on the average occupancies of the La(1), La(2), Mo(4) and Mo(5) sites. Anisotropic temperature factors were introduced for the La and Mo atoms located on the La(1), Mo(1), Mo(2), Mo(3) and Mo(4) sites and isotropic ones for the atoms occupying the other sites, with use of the weighting scheme of Killean & Lawrence (1969). The x coordinate of Mo(3) was fixed to zero to define the origin. The final reliability factors are $R = 0.038$ and $wR = 0.044$ for the 1845 main reflections used and $S = 2.13$; the largest Δ/σ values (about 0.05) are observed for the β and B thermal parameters. Refinement attempts within the *Cmca* space group led to higher agreement R factors.

It should be noted that the average structure of the crystal studied here is characterized by a pseudosymmetry in which all the O and Mo atoms of types Mo(1), Mo(2), Mo(3) occupy positions close to those found in the higher-symmetry *Cmca* space group.

Such a feature is also observed for the positions of the La(1), La(2) and Mo(4), Mo(5) sites; however, as the average occupancies P_0 of the La(1), La(2) sites by La are very different (0.842 and 0.145, respectively) and likewise for the Mo(4), Mo(5) sites (0.788 and 0.224, respectively), the departure from the higher symmetry is enhanced.

In the same way as for the $LaMo_{7.7}O_{14}$ structure, the average structure of the crystal studied can be described as derived from a hexagonal close packing of O atoms where some of them are replaced by La atoms and some oxygen vacancies are created in an ordered way. Through a period c, the O atoms of the (001) layers are stacked according to the sequence $/ABAC/A...$ (Fig. 3). The B layers ($z \simeq \frac{1}{4}$) and the C layers ($z \simeq \frac{3}{4}$) are fully occupied by O atoms of type O(2), O(3), O(4) and O(5) forming a close-packed array formulated 'O_{16}'. The A layers ($z \simeq 0$ and $z \simeq \frac{1}{2}$) include the O atoms of type O(1), O(6), O(7) and O(8). Inside these A slabs, 4 O atoms out of 16 are missing in an ordered way, half of which are replaced by La atoms, yielding a layer having the composition '$O_{12}La_2\square_2$' ($\square$ stands for the oxygen vacancies). Within this pseudohexagonal close-packing description, all the tetrahedral interstices are empty, while half of the octahedral interstices are filled by Mo atoms to give Mo_8 clusters which are formed by capping two adjacent faces of Mo_6 octahedra. The
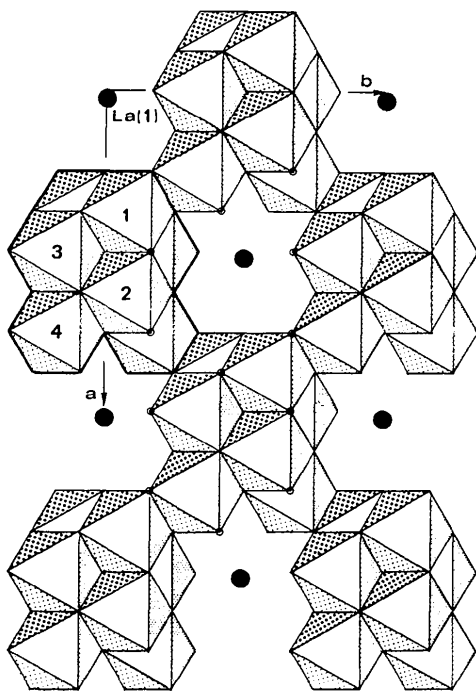
oxygen vacancies of the pseudohexagonal close-packed array occur at the centres of the Mo_6 units.

The metallic clusters are isolated and stacked in (001) layers; two adjacent layers along c are shifted by $a/2$ (or $b/2$) one with respect to the other. Let us underline the main property of the average structure. Two different configurations of the Mo_8 clusters occur: the first, which is the more likely, involves the occupancy of the Mo(4) sites, while the second implies the occupancy of the pseudoequivalent sites, i.e. the Mo(5) sites. Otherwise, a particular La site is associated with each cluster configuration, the La(1) site with the first one and the La(2) site with the second one. These two structural variants are compared in Fig. 4, with the O atoms omitted for clarity. It should be noted that, within the average structure, the atomic part including the O atoms and the Mo_6 units is the same through the two structural variants that look like 'enantiomorph' blocks.

The average distances La(1)—O, Mo(i)—O and Mo(i)—Mo(j), ($i = 1–4$ and $j = 1–4$), are very close to the related distances of the $LaMo_{7.7}O_{14}$ structure. The La atom that can occupy the La(1) or La(2) site is linked to 12 O atoms located at the corners of two types of distorted icosahedra. The La(1)—O and La(2)—O distances in these two icosahedra range from 2.44 (1) to 2.94 (1) Å and from 2.51 (1) to 2.98 (1) Å, respectively.

In the Mo_6 units, each Mo atom is linked to five O atoms located at the corners of a distorted octahedron completed with the vacant oxygen position. The Mo—O distances range from 1.99 (1) to 2.10 (1) Å. The Mo atoms located at the Mo(4) or Mo(5) sites bond with six O atoms forming distorted octahedra. The Mo(5)—O distances are rather varied [1.84 (2)

Fig. 2. A view of the $LaMo_{7.7}O_{14}$ structure. The MoO_n polyhedra are organized in Mo_8O_{24} blocks stacked in (001) layers and delimiting cavities where the La atoms are located.
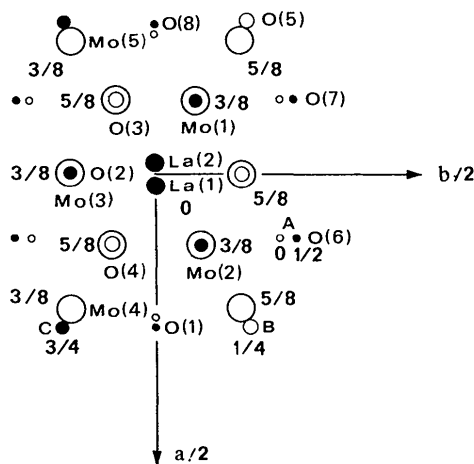

Fig. 3. A partial [001] projection of the $LaMo_8O_{14}$ average structure. A refers to the (001) oxygen layers with $z \simeq 0$ or $\frac{1}{2}$, while B and C refer to the (001) oxygen layers with $z \simeq \frac{1}{4}$ and $\frac{3}{4}$, respectively. The idealized z coordinates of Mo atoms are indicated.

to 2.23 (2) Å], in contrast with the Mo(4)—O distances [1.99 (1) to 2.04 (1) Å].

The modulated crystal

The refinement results of the average structure suggest that the satellite reflections are generated mainly through the occupancy modulation of the La(1), La(2), Mo(4) and Mo(5) sites. It is very likely that this type of modulation is closely correlated with a noticeable distortion of the basic structure, which appears as a harmonic perturbation since the second-order satellite reflections are not observed. Within this hypothesis, the displacement of the μth atom

(a)

(b)

Fig. 4. The two structural variants of the average crystal. (a) In the first variant, the Mo$_8$ clusters use the Mo(4) sites for face capping; the La(1) sites are then filled with La atoms. (b) In the second variant, the Mo(5) sites are used and associated with the La(2) sites. On each figure, only one (001) layer including Mo$_8$ clusters and La atoms is shown.

from its average position $\mathbf{r}_0^\mu + \mathbf{p}$, in the unit cell at $\mathbf{p}$, can be described by $\mathbf{U}^\mu[\mathbf{q}^* \cdot (\mathbf{r}_0^\mu + \mathbf{p})]$ where $\mathbf{q}^*$ is the modulation wavevector and $\mathbf{u}^\mu$ a periodic vector field of the internal parameters $x_4^\mu = \mathbf{q}^* \cdot \mathbf{r}_0^\mu + t$; only the t values of 0, $\frac{1}{3}$ and $\frac{2}{3}$ have to be considered since the modulation is assumed commensurate ($q_2^* = \frac{1}{3}$). The $\mathbf{U}^\mu$ components and the occupancy probabilites P^μ of sites μ by the μth atom are written as harmonic functions,

$$U_i^\mu(\bar{x}_4^\mu) = A_{i,0}^\mu + A_{i,1}^\mu \cos 2\pi \bar{x}_4^\mu + B_{i,1}^\mu \sin 2\pi \bar{x}_4^\mu,$$

where the index i refers to the axis $\mathbf{a}_i$ of the unit cell ($i = 1$, 2 or 3) and

$$P^\mu(\bar{x}_4^\mu) = P_0^\mu + C^\mu \cos 2\pi \bar{x}_4^\mu + D^\mu \sin 2\pi \bar{x}_4^\mu$$

with

$$P_0^\mu = \langle P^\mu(\bar{x}_4^\mu) \rangle.$$

The average position $\mathbf{r}_0^\mu$ of the μth atom is defined by $\mathbf{r}_0^\mu = \mathbf{r}_b^\mu + \Sigma_{i=1}^3 A_{i,0}^\mu \mathbf{a}_i$ (1), where $\mathbf{r}_b^\mu$ is the approximate average position determined from the average structure study. In the basic crystal, the La, O(1) and O(8) atoms are located at a special position, on a twofold axis; as a result, the Fourier terms of P^μ and the $\mathbf{U}^\mu$ components (de Wolff, 1977; de Wolff, Jansen & Janner, 1981) are restricted for these atoms, leading to $D^\mu = 0$; $B_{1,1}^\mu = 0$; $A_{2,0}^\mu = 0$; $A_{3,0}^\mu = 0$; $A_{2,1}^\mu = 0$; $A_{3,1}^\mu = 0$.

The refinement of the modulated structure was carried out in the superspace group $P^{C\bar{2}cq}_{\bar{1}\bar{1}\bar{1}}$ with the F magnitudes found by use of the REMOS program. The quantity minimized was $\chi^2 = (wR)^2 + (\text{p.f.})^2$, where wR is the weighted R factor and p.f. a penalty function that constrains the occupancy probabilities P^μ within reasonable ranges. Separate scale factors were introduced for the main and the satellite reflections. In the first step, only the modulation of the relevant site occupancies was considered. The refinements, with all the reflections used, were initiated by the introduction of approximate values of the Fourier coefficients C for the La(1) site and C' and D' for the Mo(4) site, which could easily be estimated from the P_0 mean values. To estimate C' and D', the P functions related to the La(1) and Mo(4) sites were assumed to be nearly in phase. This hypothesis was confirmed in the subsequent refinements. During these refinements, no constraints were applied on the mean occupancies P_0 of La(1), La(2) and Mo(4), Mo(5) sites. $P_0^{\text{La}(2)}$ and $P_0^{\text{Mo}(5)}$ were then found to be nearly equal to $1 - P_0^{\text{La}(1)}$ and $1 - P_0^{\text{Mo}(4)}$, respectively. To ensure that two adjacent La(1) and La(2) sites, which are very close, are not simultaneously occupied by an La atom, the constraint $C^{\mu'} = -C^\mu$ was applied to the Fourier coefficients of the $P^{\mu'}$ and P^μ functions. Concerning the Fourier coefficients of the P functions, related to the Mo(4) and Mo(5) sites, two models were tested: in
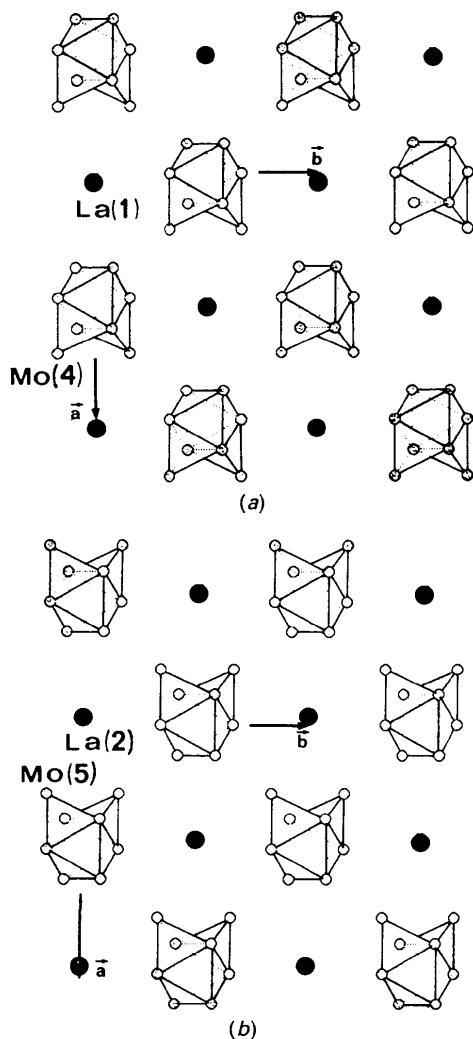
Table 2. Refinement results

$\langle x \rangle$, $\langle y \rangle$, $\langle z \rangle$ are the average atomic coordinates ($\times 10^4$) deduced from equation (1), P_0 the average occupancies ($\times 10^4$), A and B the Fourier terms ($\times 10^4$) of the modulation functions $U(\bar{x}_4)$ and $P'(\bar{x}_4)$ [the modulated part of $P(\bar{x}_4)$], β_{ij} and B_{iso} the thermal parameters ($\times 10^4$). The e.s.d.'s are in parentheses. The anisotropic thermal parameters are defined by $\exp[-(h^2\beta_{11} + k^2\beta_{22} + l^2\beta_{33} + 2hk\beta_{12} + 2hl\beta_{13} + 2kl\beta_{23})]$.

				A	B
La(1)	$\langle x \rangle$	198 (1)	U_1	12 (0)*	0
	$\langle y \rangle$	0	U_2	0	15 (1)
	$\langle z \rangle$	0	U_3	0	4 (1)
	P_0	8425 (31)	P'	1469 (15)	0
La(2)	$\langle x \rangle$	−216 (17)	U_1	−114 (33)	0
	$\langle y \rangle$	0	U_2	0	−21 (3)
	$\langle z \rangle$	0	U_3	0	22 (4)
	P_0	1450 (22)	P'	−1469 (15)	0
Mo(1)	$\langle x \rangle$	−1231 (0)	U_1	−20 (0)	−2 (0)
	$\langle y \rangle$	778 (0)	U_2	−25 (0)	16 (1)
	$\langle z \rangle$	3795 (0)	U_3	10 (0)	7 (1)
	P_0	10000			
Mo(2)	$\langle x \rangle$	1218 (0)	U_1	−23 (0)	−3 (0)
	$\langle y \rangle$	828 (0)	U_2	26 (0)	−8 (1)
	$\langle z \rangle$	3768 (0)	U_3	−8 (0)	−5 (1)
	P_0	10000			
Mo(3)	$\langle x \rangle$	0†	U_1	−22 (0)	−16 (0)
	$\langle y \rangle$	−1598 (0)	U_2	8 (1)	11 (1)
	$\langle z \rangle$	3796 (0)	U_3	0 (1)	−6 (1)
	P_0	10000			
Mo(4)	$\langle x \rangle$	2307 (1)	U_1	0 (1)	−8 (1)
	$\langle y \rangle$	−1629 (1)	U_2	2 (1)	18 (1)
	$\langle z \rangle$	3759 (0)	U_3	16 (1)	6 (1)
	P_0	7876 (34)	P'	1794 (16)	398 (12)
Mo(5)	$\langle x \rangle$	−2259 (4)	U_1	6 (7)	−13 (4)
	$\langle y \rangle$	−1608 (4)	U_2	37 (8)	−23 (4)
	$\langle z \rangle$	3835 (3)	U_3	103 (6)	−16 (4)
	P_0	2244 (24)	P'	−1794 (16)	−398 (12)
O(1)	$\langle x \rangle$	2623 (7)	U_1	14 (10)	0
	$\langle y \rangle$	0	U_2	0	−54 (12)
	$\langle z \rangle$	$\frac{1}{2}$	U_3	0	7 (14)
	P_0	10000			
O(2)	$\langle x \rangle$	−32 (6)	U_1	−36 (3)	1 (3)
	$\langle y \rangle$	−1590 (5)	U_2	−22 (11)	−13 (11)
	$\langle z \rangle$	−2362 (5)	U_3	−7 (9)	22 (11)
	P_0	10000			
O(3)	$\langle x \rangle$	−1270 (6)	U_1	−37 (4)	−14 (5)
	$\langle y \rangle$	−786 (5)	U_2	−13 (7)	5 (8)
	$\langle z \rangle$	2432 (6)	U_3	17 (7)	−1 (7)
	P_0	10000			
O(4)	$\langle x \rangle$	1158 (5)	U_1	−35 (4)	−20 (5)
	$\langle y \rangle$	−761 (5)	U_2	0 (6)	−1 (7)
	$\langle z \rangle$	2353 (5)	U_3	−21 (6)	−18 (7)
	P_0	10000			
O(5)	$\langle x \rangle$	−2557 (4)	U_1	−47 (4)	−5 (4)
	$\langle y \rangle$	1718 (5)	U_2	−9 (8)	−11 (10)
	$\langle z \rangle$	2567 (6)	U_3	45 (5)	−4 (5)
	P_0	10000			
O(6)	$\langle x \rangle$	1149 (5)	U_1	−47 (4)	11 (5)
	$\langle y \rangle$	2609 (6)	U_2	27 (6)	−4 (6)
	$\langle z \rangle$	4893 (6)	U_3	10 (7)	−14 (7)
	P_0	10000			
O(7)	$\langle x \rangle$	−1264 (5)	U_1	−36 (4)	−7 (5)
	$\langle y \rangle$	2507 (7)	U_2	−40 (7)	−1 (6)
	$\langle z \rangle$	4906 (7)	U_3	4 (8)	−14 (8)
	P_0	10000			
O(8)	$\langle x \rangle$	−2548 (7)	U_1	14 (12)	0
	$\langle y \rangle$	0	U_2	0	−38 (14)
	$\langle z \rangle$	$\frac{1}{2}$	U_3	0	−21 (17)
	P_0	10000			

	β_{11}	β_{22}	β_{33}	β_{23}	β_{31}	β_{12}
La(1)	17 (0)	18 (0)	13 (0)	−1 (0)	0	0
Mo(1)	5 (0)	11 (0)	6 (0)	0 (0)	−2 (0)	3 (0)
Mo(2)	8 (0)	11 (0)	6 (0)	1 (0)	1 (0)	−4 (0)
Mo(3)	10 (0)	5 (0)	5 (0)	0 (0)	−2 (0)	−1 (0)
Mo(4)	9 (0)	12 (0)	8 (0)	−1 (0)	−1 (0)	−1 (0)

Table 2 (cont.)

	La(2)	Mo(5)	O(1)	O(2)	O(3)
B (Å²)	0.05 (1)	0.06 (1)	0.34 (5)	0.47 (4)	0.59 (4)
	O(4)	O(5)	O(6)	O(7)	O(8)
B (Å²)	0.48 (4)	0.46 (4)	0.54 (4)	0.63 (4)	0.54 (8)

* $\sigma < 10^{-4}$.

† x coordinate of Mo(3) fixed to define the origin.

the first one, the constraints $C'^\nu = -C'^\nu$ and $D'^\nu = -D'^\nu$ were applied. In the second model, these constraints were relaxed, i.e. the coefficients C'^ν and C'^ν, D'^ν and D'^ν were disconnected. The two types of refinement led to essentially similar results within experimental error. The agreement factor for the satellite reflections was $R^1 = 0.35$ at this point.

In a second step, the Fourier terms of the U^μ components were refined, the starting values being set to zero. This refinement caused a spectacular decrease of R^1, from 0.35 to 0.09, thus confirming the existence of a displacive modulation. Anisotropic temperature factors were considered for the Mo(i) ($i = 1$ to 4) atoms and the La atom on the La(1) site, while isotropic factors were applied for the atoms on the other sites. The modulation of these factors was neglected since the observed atomic displacements were small. The weighting scheme used was $w = 100/|F_o|^2$ for $|F_o| > |F_{min}|$, $w = 100/|F_{min}|^2$ for $|F_o| < |F_{min}|$, with $|F_{min}| = 100$. The global agreement factor is $R = 0.051$, the partial R factors related to the (1845) main reflections and (1502) satellite reflections are $R^0 = 0.038$ and $R^1 = 0.090$, respectively; the corresponding weighted factors are $wR = 0.070$, $wR^0 = 0.054$ and $wR^1 = 0.110$; $S = 0.43$; $(\Delta/\sigma)_{max} = 0.05$ (on β and B).

Discussion

Modulation features and symmetry

The refinement results given in Table 2 show that the La, Mo and O atoms, which occupy the same sites as in the $LaMo_{7.7}O_{14}$ crystal, experience only small displacements from their basic positions, less than about 0.05 Å. In contrast, the La atom on the La(2) site and the Mo atom on the Mo(5) site undergo noticeable displacements along a (maximal value of 0.13 Å) and along c (maximal value of 0.10 Å), respectively, and, furthermore, these displacements are nearly in opposition. Within experimental error, the P_0 mean occupancies (Table 3) of the La(1) and La(2) sites are complementary, as are those for the Mo(4) and Mo(5) sites. This results in a stoichiometric composition for the crystal, $LaMo_8O_{14}$, in contrast with the nonmodulated phase, which has the formula $LaMo_{7.7}O_{14}$. The P occupancies of the La(1) and Mo(4) sites as well as those of the La(2) and Mo(5) sites appear to be strongly correlated (Tables 2 and 3): when the La atoms occupy the La(1) sites,

Table 3. *Variation of the interatomic distances* (Å) *along* [010] (*e.s.d.'s in parentheses*)

For a given atomic pair, the distances are written on the same line and their sequence along [010] defined by referring to the basic crystal through the symbols 2 (twofold axis) or c (glide plane), on the top line. The symmetry code used in the first column also refers to the basic crystal: (i) x, $-y$, $-z$; (ii) $\frac{1}{2}+x$, $\frac{1}{2}+y$, z; (iii) $\frac{1}{2}+x$, y, $\frac{1}{2}-z$; (iv) x, $\frac{1}{2}-y$, $\frac{1}{2}+z$; (v) x, $\frac{1}{2}+y$, $\frac{1}{2}-z$; (vi) $\frac{1}{2}+x$, $\frac{1}{2}-y$, $-z$. The occupancy probabilities P of the La(1), La(2) and Mo(4), Mo(5) sites, calculated from the results of Table 2, are also given; the standard deviations on the P values are less than 0.004.

(a) Mo—Mo distances in the metallic clusters of the same (001) layer

	2	c	2	c	2	c	2
Mo(1)—Mo(1ⁱ)	2.670 (1)		2.691 (2)		2.733 (2)		2.754 (1)
Mo(1)—Mo(2)		2.724 (2)	2.726 (2)	2.724 (2)	2.728 (2)	2.727 (2)	2.729 (2)
Mo(1)—Mo(3)		2.723 (2)	2.726 (2)	2.740 (2)	2.747 (2)	2.760 (2)	2.763 (2)
Mo(1ⁱ)—Mo(3)		2.733 (2)	2.733 (2)	2.735 (2)	2.735 (2)	2.737 (2)	2.737 (2)
Mo(1)—Mo(5)		2.58 (1)	2.64 (1)	2.58 (1)	2.71 (1)	2.66 (1)	2.72 (1)
Mo(1ⁱ)—Mo(5)		2.49 (1)	2.55 (1)	2.55 (1)	2.66 (1)	2.66 (1)	2.71 (1)
Mo(2)—Mo(3)	2.850 (1)		2.830 (2)		2.786 (2)		2.766 (1)
Mo(2)—Mo(3)		2.793 (1)	2.778 (2)	2.795 (2)	2.765 (2)	2.780 (2)	2.766 (1)
Mo(2ⁱ)—Mo(3)		2.725 (2)	2.734 (2)	2.724 (2)	2.741 (2)	2.731 (2)	2.739 (2)
Mo(2)—Mo(4)		2.778 (2)	2.733 (2)	2.786 (2)	2.694 (2)	2.745 (2)	2.702 (2)
Mo(2ⁱ)—Mo(4)		2.705 (2)	2.684 (2)	2.724 (2)	2.680 (2)	2.720 (2)	2.698 (2)
Mo(3)—Mo(4)		2.588 (2)	2.593 (2)	2.565 (2)	2.571 (2)	2.544 (2)	2.548 (2)
Mo(3)—Mo(5)		2.49 (1)	2.49 (1)	2.51 (1)	2.52 (1)	2.54 (1)	2.54 (1)

(b) Mo—Mo distances between the metallic clusters of the same (001) layer

	2	c	2	c	2	c
Mo(4)—Mo(5ᵛⁱ)	2.821 (7)	2.830 (8)	2.870 (6)	2.880 (6)	2.923 (8)	2.928 (7)
Mo(1ⁱ)—Mo(4ᵛⁱ)	3.083 (2)	3.074 (2)	3.070 (2)	3.053 (2)	3.050 (2)	3.041 (2)
Mo(2ⁱ)—Mo(5ᵛⁱ)	3.079 (8)	3.107 (9)	3.046 (7)	3.103 (7)	3.043 (9)	3.071 (8)

(c) La—O distances

	2	c	2	c	2	c	2
La(1)—O(1ⁱⁱⁱ)	2.86 (2)		2.86 (2)		2.87 (2)		2.87 (2)
La(1)—O(2)		2.73 (1)	2.73 (1)	2.71 (1)	2.70 (1)	2.69 (1)	2.68 (1)
La(1)—O(3)		2.93 (1)	2.92 (1)	2.89 (1)	2.87 (1)	2.85 (1)	2.84 (1)
La(1)—O(4)		2.50 (1)	2.49 (1)	2.54 (1)	2.53 (1)	2.58 (1)	2.57 (1)
La(1)—O(6ⁱᵛ)		2.57 (1)	2.59 (1)	2.59 (1)	2.64 (1)	2.64 (1)	2.67 (1)
La(1)—O(7ⁱᵛ)		3.03 (1)	3.04 (1)	2.97 (1)	2.99 (1)	2.91 (1)	2.93 (1)
La(1)—O(8ⁱⁱⁱ)	2.51 (2)		2.51 (2)		2.51 (2)		2.51 (2)
$P^{\text{La}(1)}$	0.987		0.915		0.768		0.695
La(2)—O(1ⁱⁱⁱ)	2.26 (4)		2.33 (3)		2.48 (3)		2.55 (4)
La(2)—O(2)		2.73 (1)	2.72 (1)	2.72 (1)	2.69 (1)	2.69 (1)	2.68 (1)
La(2)—O(3)		2.63 (2)	2.63 (2)	2.65 (2)	2.65 (2)	2.67 (2)	2.67 (2)
La(2)—O(4)		2.80 (3)	2.74 (2)	2.82 (2)	2.70 (2)	2.78 (2)	2.72 (2)
La(2)—O(6ⁱᵛ)		2.85 (2)	2.81 (2)	2.87 (2)	2.80 (2)	2.85 (2)	2.81 (2)
La(2)—O(7ⁱᵛ)		2.75 (2)	2.76 (2)	2.74 (2)	2.77 (2)	2.75 (2)	2.77 (2)
La(2)—O(8ⁱⁱⁱ)	3.11 (4)		3.04 (3)		2.89 (3)		2.83 (4)
$P^{\text{La}(2)}$	0		0.071		0.218		0.292

(d) Mo—O distances

	2	c	2	c	2	c	2
Mo(1)—O(2ⁱ)	2.05 (1)	2.06 (1)	2.03 (1)	2.06 (1)	2.03 (1)	2.04 (1)
Mo(1)—O(3)	2.00 (1)	2.01 (1)	1.99 (1)	2.02 (1)	2.00 (1)	2.02 (1)
Mo(1)—O(5)	2.09 (1)	2.10 (1)	2.08 (1)	2.09 (1)	2.07 (1)	2.07 (1)
Mo(1)—O(7)	1.99 (1)	2.01 (1)	1.99 (1)	2.03 (1)	2.01 (1)	2.03 (1)
Mo(1)—O(8)	1.95 (1)	1.97 (1)	1.98 (1)	2.01 (1)	2.03 (1)	2.04 (1)
Mo(2)—O(1)	2.15 (1)	2.10 (1)	2.14 (1)	2.06 (1)	2.10 (1)	2.06 (1)
Mo(2)—O(2ⁱ)	2.04 (1)	2.07 (1)	2.03 (1)	2.07 (1)	2.03 (1)	2.06 (1)
Mo(2)—O(4)	2.08 (1)	2.07 (1)	2.07 (1)	2.05 (1)	2.04 (1)	2.03 (1)
Mo(2)—O(5ⁱⁱⁱ)	2.03 (1)	2.04 (1)	2.03 (1)	2.05 (1)	2.05 (1)	2.06 (1)
Mo(2)—O(6)	2.06 (1)	2.07 (1)	2.05 (1)	2.07 (1)	2.05 (1)	2.06 (1)
Mo(3)—O(2ⁱᵛ)	2.08 (1)	2.10 (1)	2.08 (1)	2.13 (1)	2.10 (1)	2.12 (1)
Mo(3)—O(3)	2.06 (1)	2.05 (1)	2.07 (1)	2.05 (1)	2.07 (1)	2.06 (1)
Mo(3)—O(4)	2.03 (1)	2.03 (1)	2.03 (1)	2.03 (1)	2.03 (1)	2.03 (1)
Mo(3)—O(6ⁱ)	2.03 (1)	2.03 (1)	2.03 (1)	2.03 (1)	2.03 (1)	2.03 (1)
Mo(3)—O(7ⁱ)	2.06 (1)	2.05 (1)	2.07 (1)	2.04 (1)	2.07 (1)	2.06 (1)
Mo(4)—O(1)	2.02 (1)	1.97 (1)	2.07 (1)	1.97 (1)	2.07 (1)	2.02 (1)
Mo(4)—O(3ⁱⁱⁱ)	2.08 (1)	2.08 (1)	2.10 (1)	2.10 (1)	2.12 (1)	2.12 (1)
Mo(4)—O(4)	2.06 (1)	2.06 (1)	2.02 (1)	2.01 (1)	1.97 (1)	1.97 (1)
Mo(4)—O(5ⁱⁱ)	1.97 (1)	2.00 (1)	1.97 (1)	2.01 (1)	1.99 (1)	2.01 (1)
Mo(4)—O(6ⁱ)	2.07 (1)	2.08 (1)	2.04 (1)	2.04 (1)	2.01 (1)	2.01 (1)
Mo(4)—O(7ⁱⁱ)	2.08 (1)	2.08 (1)	2.10 (1)	2.10 (1)	2.11 (1)	2.11 (1)
$P^{\text{Mo}(4)}$	0.944	0.950	0.781	0.794	0.626	0.632
Mo(5)—O(3)	1.89 (2)	1.90 (2)	1.88 (2)	1.90 (2)	1.88 (2)	1.89 (2)
Mo(5)—O(4ⁱⁱⁱ)	2.30 (2)	2.28 (2)	2.26 (2)	2.22 (2)	2.20 (2)	2.18 (2)

Table 3 (cont.)

	2	c	2	c	2	c	2
Mo(5)—O(5ⁱ)	2.26 (2)	2.23 (2)	2.17 (2)	2.11 (2)	2.05 (2)	2.02 (2)	
Mo(5)—O(6ⁱⁱ)	2.19 (2)	2.17 (2)	2.19 (2)	2.14 (2)	2.17 (2)	2.15 (2)	
Mo(5)—O(7ⁱ)	1.76 (2)	1.77 (2)	1.83 (2)	1.85 (2)	1.91 (2)	1.92 (2)	
Mo(5)—O(8)	1.87 (2)	1.88 (2)	1.96 (2)	1.96 (2)	2.04 (2)	2.05 (2)	
$P^{Mo(5)}$	0.068	0.062	0.230	0.218	0.386	0.380	

the Mo(4) sites are more likely to be filled by the Mo atoms. A similar phenomenon occurs for the La(2) and Mo(5) sites. However, since the average occupancy of the La(1) site is larger than that of the Mo(4) site (Table 2), the La and Mo atoms must occupy two neighbouring La(1) and Mo(5) sites in some parts of the crystal.

Because the modulated structure is assumed to be commensurate, the actual atomic scheme can be described either on the basis of a superspace group or in the context of a conventional space group. It is verified that the atomic displacements U, deduced from the symmetry operators of $P^{C2ca}_{\bar{1}\bar{1}1}$, are consistent, within the basis $\mathbf{a}$, $3\mathbf{b}$, $\mathbf{c}$, with the space group $P2na$, which is a subgroup of $C2ca$. Consequently, if the basis $\mathbf{a}$, $\mathbf{b}$, $\mathbf{c}$ is chosen as the reference basis, the study of the interatomic distances can be limited to the appropriate x and y intervals $-\frac{1}{4}$, $\frac{1}{4}$ and 0, $\frac{3}{2}$, respectively. The variations of the main interatomic distances, along [010], are shown in Table 3 for the La—O, Mo—O bonds and the Mo—Mo bonds in the metallic clusters. Running along $\mathbf{b}$, from 0 to $\frac{3}{2}$ (a, b, c basis), four independent metallic clusters, as well as four distinct LaO₁₂ polyhedra, for each type of site La(1) and La(2), are found in the actual crystal. Within two of these atomic blocks a symmetry about a twofold axis is involved (for $y = 0$ and $y = \frac{3}{2}$), while within the two other atomic blocks the binary symmetry is lost.

The displacements of the atoms, from their basic positions, display remarkable properties. Let us consider two atoms A and B of the same kind and two atoms C and D of the same kind along $\mathbf{b}$ (see Fig. 5)
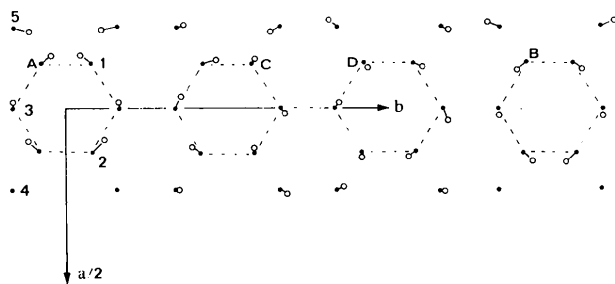
Fig. 5. The displacive modulation within the metallic clusters. [001] projection. The average positions of Mo are indicated with black spots, their actual positions by open circles; the displacements are magnified disproportionately for clarity. The dotted lines define the Mo₆ octahedra.

whose y coordinates are related by $\langle y_B \rangle - \langle y_A \rangle = \frac{3}{2}$ and $\langle y_C \rangle + \langle y_D \rangle = \frac{3}{2}$. Their displacements U_1, U_2, U_3 along the $\mathbf{a}$, $\mathbf{b}$ and $\mathbf{c}$ axes are correlated in a remarkable way: in the first case $U_1^B = -U_1^A$, $U_2^B = -U_2^A$ and $U_3^B = U_3^A$, while in the second case $U_1^D = -U_1^C$, $U_2^D = U_2^C$ and $U_3^D = -U_3^C$. This property, illustrated in Fig. 5, with the displacements of the Mo atoms within the metallic clusters taken as an example, is the result of both the symmetry operators of the superspace group and the particular rational value $\frac{1}{3}$ of q_2^*. Within a classical approach, $i.e.$ with use of the $P2na$ space group, the relation between the previous displacements would be masked.

The evolution of the metal–oxygen bonds

The variations of the La—O distances, related to the O atoms of type O(2), O(3), O(4), O(6) and O(7), are smooth and of the same order of magnitude at the La(1) and the La(2) sites (Table 3). The two other La—O distances are related to the O atoms of type O(1) and O(8) and vary widely and in opposite directions on the La(2) sites while the homologous distances on the La(1) sites are nearly constant. As a result, the La environment is nearly similar for the four independent La(1) sites: the La(1)—O distances range from 2.50 (1) to 3.03 (1) Å when the occupancy probability $P^{La(1)}$ is largest (0.987) and from 2.51 (2) to 2.93 (1) Å when $P^{La(1)}$ is smallest (0.695). When the La atom is likely to occupy the La(2) sites, for $P^{La(2)} = 0.292$, the La(2)—O distances range from 2.55 (4) to 2.83 (4) Å, which represents a significantly smaller spread than the La(1)—O distances.

The variations of the Mo(i)—O distances ($i = 1$ to 4) are small, less than 0.1 Å (Table 3c). As a result, the surroundings of these Mo atoms are nearly similar to those observed in the LaMo₇.₇O₁₄ crystal. In contrast, four out of six Mo(5)—O distances vary greatly, the largest variation reaching 0.24 Å, leading to the following property: the Mo(5)—O distances range from 1.76 (2) to 2.30 (2) Å when the occupancy probability P of the Mo(5) site is smallest (≈ 0.06), while the dispersion of these distances is considerably less, 1.89 (2) to 2.18 (2) Å, in the configuration where P is the largest (≈ 0.38). Otherwise, when Mo is likely to occupy the Mo(5) site ($P \geq 0.20$), it forms two bonds (≈ 1.9 Å) with O atoms that are stronger than the homologous bonds found in the Mo(4) O₆ octahedra (Table 3c).

The calculation of the oxidation states of Mo atoms from the bond-length–bond-strength formula of Brown & Wu (1976) for the Mo—O bonds (1.882/$d_{Mo—O}$)$^{+6.0}$ leads to the following results: the summation of the assessed valences within the independent MoO$_n$ ($n = 5$ or 6) polyhedra of the actual crystal, with the P values taken into account, is equal to 76.9 for 24 Mo, which compares favourably with the value of 75 deduced from the chemical formula.

The calculated oxidation states of Mo(2), Mo(3) and Mo(4) atoms show only a small variation, their range of values being 2.83–2.97, 2.92–2.99 and 3.63–3.76, respectively. In contrast, the variation of oxidation states of Mo(1) and Mo(5) atoms is quite large. Along **b**, from 0 to $\frac{3}{2}$, the valence sums for Mo(1) and Mo(5) atoms decrease from 3.34 to 3.08 and from 4.53 to 3.97, respectively. This phenomenon seems to be correlated with the occupancy probability of the Mo(5) site, which increases with y in the above interval.

The metallic clusters

Let us first present a few observations regarding the Mo—Mo distances within the metallic clusters. The distances Mo(1)—Mo(1^i) and Mo(2)—Mo(2^i) (Table 3a), which correspond to the opposite edges in the Mo$_6$ octahedra, vary moderately but in opposite directions along **b**. The variation amplitudes of these distances are the same (about 0.08 Å). Large variations, up to 0.22 Å, are observed for the Mo(1)—Mo(5) and Mo(1^i)—Mo(5) distances, while variations in the homologous distances, involving the Mo(4) sites, are less than 0.1 Å. As in LaMo$_{7.70}$O$_{14}$, the strongest Mo—Mo bonds are observed between Mo(3) and the atoms that cap the faces of the Mo$_6$ units, in this case Mo(4) and Mo(5), respectively.

Within a given cluster, the Mo(4) and Mo(5) sites of the same coordinate y cannot be filled simultaneously by Mo atoms. Indeed, in all the unit cells, the occupancy probabilities P of these sites are found to be nearly complementary (Table 3c). Otherwise, if these sites were both to be occupied, unrealistically short distances for Mo(4)—Mo(5^{iii}) would result (from 2.33 to 2.55 Å), with the assumption of $P2na$ symmetry. Consequently, the previous result and the chemical formula LaMo$_8$O$_{14}$ require that all the clusters are Mo$_8$ clusters.

In the region of the crystal defined by $y = 3n$ (n integer; basis **a**, **b**, **c**) effectively only one configuration is found for the Mo$_8$ cluster. This is the *cis*-edge-sharing cluster shown in Fig. 6(a), which uses the Mo(4) sites for the face capping, as is found in LaMo$_{7.70}$O$_{14}$. In the region of the crystal defined by $y = n + \frac{3}{2}$, two configurations are possible, one of which is again given in Fig. 6(a), while the other is shown in Fig. 6(b). The latter has a point symmetry similar to

Fig. 6(a) but is oriented differently and uses the Mo(5) positions for the capping atoms. It will occur with a reduced probability, $P = 0.38$, as compared with that for Fig. 5(a), $P = 0.62$. Each of these configurations is governed by a binary symmetry.

In other regions of the crystal the occupancy probabilities of the two neighbouring Mo(4) [or Mo(5)] sites are distinctly different (Table 3c), in agreement with the absence of a twofold axis. The distribution of the P values along [010] implies the following results: in the regions of the crystal defined by $y = 3n + \frac{1}{2}$ and $y = 3n + 1$, at least three configurations are possible for the Mo$_8$ clusters (Figs. 6a–6c). However, the configuration of Fig. 6(d) cannot be rejected, although it appears less likely than that of Fig. 6(c). In the regions defined by $y = 3n + \frac{5}{2}$ and $y = 3n + 2$, the cluster configurations are symmetric with the previous ones with respect to the twofold axis located at $y = 3n + \frac{3}{2}$. So, in these regions, the configuration of Fig. 6(d) is more likely to occur than that of Fig. 6(c).

In summary, then, four distinct configurations of the Mo$_8$ clusters, two each of the two different isomeric forms, are likely to occur throughout the crystal with significant probabilities. So far as we are aware, the *cis*-edge-sharing isomer has been observed in chemical systems only for LnMo$_{8.}$O$_{14}$ (Ln = Ce, La, Pm, Nd, Gd) (Leligny *et al.*, 1990; Gougeon & McCarley, 1991). On the other hand, the *trans* isomer of the metal cluster has been observed in certain coordination complexes such as Re$_8$C(CO)$_{24}$ (Ciani, D'Alfonso, Freni, Romiti & Sironi, 1982).
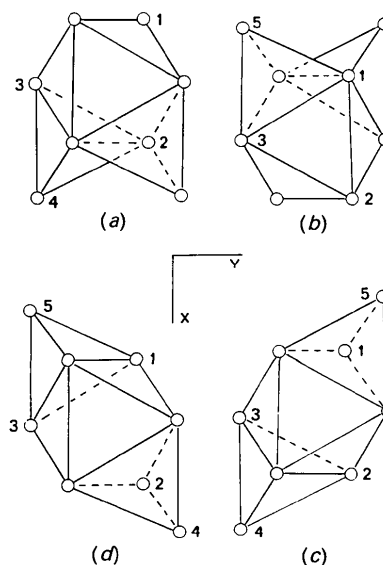

Fig. 6. (a)–(d) The four possible configurations of the Mo$_8$ metallic clusters in the actual crystal. The configuration (a) is favoured. See text for further details.

The broadening of satellite spots: electron microscopy study

As pointed out above, the satellite spots exhibit abnormal features. This suggests a significant perturbation with respect to the ideal modulation described for this crystal. To understand this phenomenon, an electron microscopy investigation was performed on several microcrystals of the same batch of nominal composition $LaMo_8O_{14}$.

The samples, picked up from the single-crystal preparation used for X-ray study, were crushed in alcohol. The microcrystals were suspended and deposited in a holey carbon film. The electron microscopy study was performed with a JEOL 200 CX electron microscope equipped with a side-entry goniometer ($\pm 60°$) operating at 200 kV.

The electron diffraction study showed that all the microcrystals were characterized by the same ortho-rhombic subcell with $a \approx 11.1$, $b \approx 10.0$, $c \approx 9.2$ Å. Some of these crystals display only main reflections and can be identified as having the $LaMo_{7.7}O_{14}$-type structure. However, the electron diffraction patterns of most of the crystals exhibit satellite reflections along the b^* axis, as shown from Fig. 7. In every modulated crystal, the satellite spots are broadened along b^* and merged in diffuse [010]* streaks. The measurements carried out on several crystals show that the q_2^* component of the modulation wave-vector varies slightly from one crystal to the other from about 0.33 to 0.37. These values are close to the ideal value of $\frac{1}{3}$. These results can be considered to be consistent with the previous X-ray diffraction study.

The bright-field images (Fig. 8) recorded from different crystals reveal additional important features. An even contrast, distributed in an uniform way with a periodicity of 5 Å, is observed for the nonmodulated crystals while a striped contrast (Fig. 8a) is observed for most of the modulated crystals. This striped contrast is characterized by the alter-nation of two dark fringes with groups of three to

five bright fringes, *i.e.* varying about the mean of four. The average period of this alternation appears to be equal to the period (30 Å) of the modulation observed in X-ray patterns. Two other significant results should be pointed out: (i) several modulated crystals exhibit large regions of even contrast coexis-ting with regions of striped contrast (Fig. 8b); (ii) the intensities of the satellite reflections as well as those of the streaks vary from one crystal to the other. An intensity increase of the diffuse streaks is associated with an intensity decrease of the satellite spots. It is observed that this phenomenon is related to a larger irregularity of the fringe alternation. The result (i) suggests that both modulated and nonmodulated zones could be found in the same crystal. The result (ii) could be related to the ratio of the two zone types (and/or) to the more or less large deviation from an ideal structural order. The irregularity of the fringe alternation along **b** is consistent with such a devia-tion, which would give rise to the diffuse [010]* steaks and the broadening of the satellite spots. A possible variation of q_2^* within the same crystal cannot be rejected but does not allow one to explain the large angular spread of the satellite reflections. Indeed, for a maximum variation of q_2^* equal to 0.04, the θ variation of the 1121 satellite reflection, for instance, is about 0.04°. Finally, the unusual
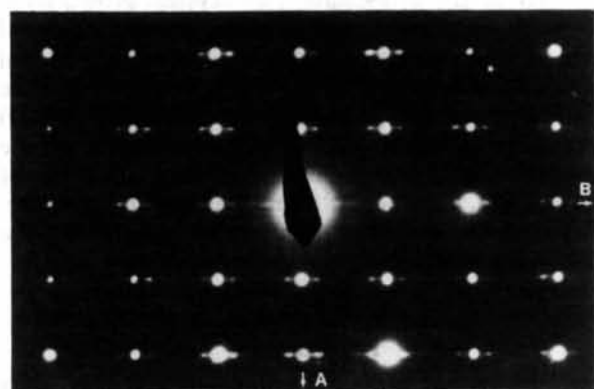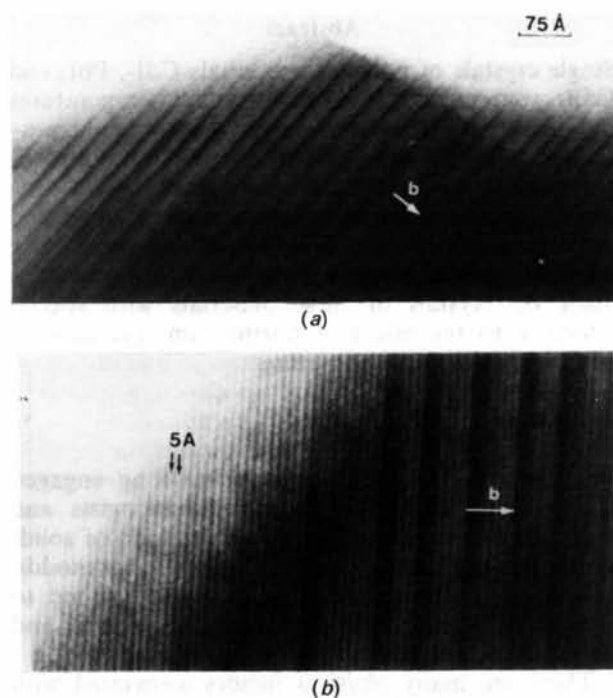

(a)

(b)

Fig. 8. [001] bright-field images. (a) The modulated phase exhibits a striped contrast arising from the alternation of two dark and several bright fringes. (b) In some crystals, large domains appear as nonmodulated regions (left part of the micrograph).

Fig. 7. [001] electron diffraction pattern of the modulated phase.

features observed for the satellites may be related to a pseudoperiodic distribution of the different types of Mo$_8$ clusters along **b**. In spite of this deviation from an ideal modulated crystal, it seems reasonable to assume that the refinement results reported here give the main features of the structure without noticeable bias.

The authors are grateful to Mrs R. Aguinet and Mrs J. Chardon for their technical assistance.

References

B. A. FRENZ & ASSOCIATES, INC. (1982). *SDP Structure Determination Package.* College Station, Texas, USA.

BROWN, I. D. & WU, K. K. (1976). *Acta Cryst.* B32, 1957–1959.
CIANI, P., D'ALFONSO, G., FRENI, M., ROMITI, P. & SIRONI, A. (1982). *J. Chem. Soc. Chem. Commun.* p. 705.
DOUDIN, B. (1985). Private communication.
GOUGEON, P. & MCCARLEY, R. E. (1991). *Acta Cryst.* C47, 241–244.
KILLEAN, R. C. G. & LAWRENCE, J. L. (1969). *Acta Cryst.* B25, 1750–1752.
LELIGNY, H., LEDESERT, M., LABBE, P., RAVEAU, B. & MCCARROLL, W. H. (1990). *J. Solid State Chem.* 87, 35–43.
SMAALEN, S. VAN, (1987). *Acta Cryst.* A43, 202–207.
WOLFF, P. M. DE (1977). *Acta Cryst.* A33, 493–497.
WOLFF, P. M. DE, JANSEN, T. & JANNER, A. (1981). *Acta Cryst.* A37, 625–636.
YAMAMOTO, A. (1982). *REMOS.* A computer program for the refinement of modulated structures. National Institute for Research in Inorganic Materials, Niiharigun Ibaraki, Japan.

Impurity- and Temperature-Dependent Structural Transformations in Polytypic Crystals of CdI₂, PbI₂ and CdBr₂

BY S. K. CHAUDHARY

Department of Physics, University College, M. D. University, Rohtak 124001, India

Abstract

Single crystals of polytypic materials CdI₂, PbI₂ and CdBr₂ were purified and grown at high temperatures by use of zone-refinement and Bridgman–Stockbarger techniques. The crystals were investigated by X-ray diffraction to ascertain how the purification of crystals influences the growth and polytypism of crystals. The results obtained were compared and correlated with various other studies made on crystals of these materials with special reference to the effect of purification, presence of impurities and the temperature.

Introduction

The phenomenon of polytypism has long engaged the attention of physicists and mineralogists and more recently it has attracted the attention of solid-state physicists because various polytypic modifications of the same substance have been found to possess different semiconducting, dielectric and photovoltaic properties (Tairov & Tsvetkov, 1983).

There are many physical factors associated with the growth of polytypes and a large number of explanations have been put forward to account for the phenomenon (Trigunayat & Verma, 1976). These have been based on such diverse considerations as temperature, rate of crystallization, presence of impurities, thermodynamical factors, creation of dislocations during growth, internal rotations, electron energy *etc.* Of these, the presence of impurities is prominent and plays an important role in the growth and phase transformations of polytypes (Jepps & Page, 1984).

In the past three decades a considerable amount of work has been performed on the polytypism of CdI₂, PbI₂ and CdBr₂ crystals grown from solution, vapour or gel. Whereas this work has yielded significant results, not much attention has been paid thus far to the investigation of crystals grown from melt. The zone-refinement technique was employed here so that the degree of purification of the material could be controlled and single crystals of the material could be grown. X-ray diffraction (XRD) *was used to study the nature of growth of the polytypes* with special reference to the effects of purification, presence of impurities and temperature. The results are compared with others in the literature.

Experimental

The details of the zone-refinement system and growth processes of CdI₂ and PbI₂ crystals have been